ICAS-96-4.10.4

MEASUREMENTS OF THE PROPELLER SLIPSTREAM INTERACTION WITH A NACELLE AND WING

D. J. Barber* T. E. Nelson†

de Havilland Inc.
Garratt Blvd., Downsview, Ontario
Canada M3K 1Y5

Abstract

Flow field and surface pressure measurements of the interaction of a propeller slipstream with a nacelle and wing are presented. The slipstream is shown to strongly affect the local wing loading. Wing local lift coefficient data from the integration of wing surface pressures are related to a propeller slipstream parameter, C_P/J^2. Flow field surveys of total pressure coefficient and cross-flow velocity vectors are presented. These data were acquired at six stations downstream of a six-bladed propeller using a five-hole probe. Measurements were taken for two angles of attack, zero and five degrees. These two cases represent a cruise case and a takeoff or climb case for a turboprop aircraft. The measurements are at a higher propeller power loading than previous results and are representative of the next generation of turboprop aircraft. Data from the cruise case show a nearly uniform distribution of total pressure coefficient with significant levels of swirl. Data from the takeoff climb case show an asymmetric distribution of total pressure with high levels of swirl. These data provide a necessary basis for CFD code validation and correlation work on high performance turboprop aircraft.

Nomenclature

C_P	power coefficient $= P/(\rho_\infty n^3 D^5)$
C_p	pressure coefficient $= (p - p_\infty)/q_\infty$
C_{pt}	total pressure coefficient $= (p_t - p_\infty)/q_\infty$
C_T	thrust coefficient $= T/(\rho_\infty n^2 D^4)$
D	propeller diameter = 2 ft
J	advance ratio $= U_\infty/(nD)$
N	propeller RPM
P	propeller shaft power
T	propeller thrust
U_∞	freestream velocity
b	wing span = 6 ft.
c	wing chord = 18.375 in
p	static pressure
p_t	total pressure
q_∞	freestream dynamic pressure $= \frac{1}{2}\rho_\infty U_\infty^2$
y	spanwise coordinate
α	angle of attack
β	propeller pitch angle
ρ_∞	freestream density

Introduction

A complete turboprop wing-mounted engine installation presents a challenge for aerodynamic analysis and modeling. Understanding the installation effects is necessary to predict aircraft flight dynamics and performance. The combination of a propeller slipstream and an asymmetric nacelle mounted on a wing creates a complex flow field for both aver-

*Principal Engineer.
†Senior Engineer.

aged and unsteady flow terms. The wing and nacelle introduce a nonsymmetric inflow field for the propeller and the wing experiences a non-symmetric inflow field from the propeller slipstream. Steady and time-varying loads on the propeller, nacelle and wing can be important.

The objective of this experiment was to develop a better understanding of the aerodynamics of a turboprop engine installation and to provide data for CFD code development and validation.

Previous experimental measurements of propeller slipstreams includes the work of Samuelsson [1] and Aljabri [2]. At de Havilland Inc., earlier research on propeller installation effects has been presented by Eggleston [3] and Smith [4].

The wind-tunnel model used here represents a complete turboprop engine installation. The nacelle was mounted on a two-dimensional wing and included intake and exhaust systems. A six-bladed propeller, driven by an electric motor, was utilized for the experiment.

Five-hole probe measurements are presented at two conditions, cruise and a takeoff climb. For the cruise condition, the angle of attack was 0 degrees and the Mach number was 0.294. The propeller advance ratio was 3.2 and the power coefficient was 1.6, resulting in significant swirl in the propeller slipstream. For the takeoff climb case the Mach number was 0.175 and the angle of attack was 5 degrees, resulting in significant asymmetric loading. The advance ratio was 1.0 and the power coefficient was 0.4, resulting in high slipstream swirl. These two conditions are typical of a cruise case and a takeoff climb case for a new generation of high-speed turboprop regional aircraft.

Wind-Tunnel Model

Model Description

A quasi-two-dimensional wind-tunnel model approximately one fifth full scale was used for the investigation. The model consisted of a two-dimensional wing with a complete powered model of a turboprop nacelle, mounted mid span.

The wing was an 18% thick section used on the Dash 8 series of aircraft. It was constructed of molded epoxy on a 4×8 inch steel box beam 0.5 inch thick. The wing featured detachable leading and trailing edges for housing nacelle utilities and electronic scanning modules.

The powered nacelle drove a 2 foot diameter carbon fiber propeller with six blades which were manually adjustable in pitch. The propeller was designed for power levels and rotational speeds appropriate to the new, faster and more powerful turboprop applications with cruise thrust and power coefficients coefficients above 0.35 and 1.5 respectively. The propeller blades were designed with an activity factor of 140 per blade. Contemporary sections were utilized for the design and these sections were developed and tested by de Havilland Inc [3].

The nacelle was rectangular in cross-section with rounded shoulders and featured a pitot intake. The nacelle dimensions were 8 inches wide, 11 inches deep and approximately 64 inches long. A centerline cross-section is shown in Figure 1. The nacelle includes an air intake system and a powered exhaust system for simulation of a complete turboprop installation. Intake air was controlled by a perforated plate at the rear of the intake duct to obtain the appropriate inlet velocity ratio. The exhaust system used the intake air in combination with an ejector. The ejector was driven by compressed air to energize the exhaust to the appropriate pressure ratio and exit Mach number.

The nacelle also housed the 100 HP electric motor for the propeller drive, along with a water cooling system for the motor. The motor was driven by a 3-phase, variable frequency 175 kva solid state inverter which provided speed control within 0.1%.

Instrumentation

The wing was instrumented with two chordwise rows of 72 surface pressure taps, located 8.4 in. either side of the nacelle centerline. This corresponds to 70% of the propeller radius. Additional spanwise rows of 12 pressure taps were located at $x/c = 0.030$ and $x/c = 0.167$ on the upper surface of the wing.

The nacelle forebody was instrumented with 158 pressure taps, some being used to determine intake flow, inlet losses and distortion levels. The intake

lips contained surface pressure taps to assess sensitive locations about the inlet.

The nacelle aftbody featured 31 surface pressure taps on the sides and lowest buttline. Additional taps were placed at the exhaust exit for measurement of the exhaust conditions.

Electronic scanning modules were housed within the wing leading and trailing edges and in the forebody and aftbody of the nacelle. Six scanning modules were used with a total of the 256 5-psi transducers.

Propeller instrumentation comprised of a six-component rotating balance mounted within the propeller hub. Balance signals and power supply were provided by a close-coupled telemetry system, mounted ahead of the electric motor. Propeller speed was monitored through an optical pickup, mounted about a 256 toothed wheel on the propeller shaft. The acquisition of unsteady pressure data and propeller balance data was triggered from this optical pickup. Another optical pickup provided an index pulse, once per revolution.

A variety of probes were used with the traversing rig, including pitot-static tubes, a high-response pitot tube and a five-hole probe. The five-hole probe was precalibrated over a range of Mach number, pitch angle and yaw angle. Pressures were measured using 5 calibrated pressure transducers which were referenced to the wind-tunnel static pressure.

Test Description

Initial Testing

Preparatory testing was completed prior to the test described here. In order to accurately determine slipstream losses and the source of losses for a complete nacelle installation, these calibrations were required. The isolated propeller was calibrated on a separate test rig with an axisymmetric nacelle. The range of blade angles and operating conditions to be utilized were tested. Included were the takeoff climb and cruise conditions. Additional tests were carried out with a similar asymmetric nacelle featuring a pitot inlet. These tests considered the nacelle without the wing present. A range of inflows and blade angles were tested. These tests established the baseline propeller performance and the impact of a typical nacelle on that performance.

Experimental Technique

In order to study the flow field, a five-hole probe was utilized. From the outset, it was recognized that a technique allowing high-speed acquisition over a large number of locations was necessary to describe the flow. The wind tunnel was equipped with a five-axis traverse which is computer controlled and allows the mounting of a discrete non-intrusive probe for flow measurement. Positioning and data acquisition proved achievable at the rate of one data point every 3 seconds.

Since one of the primary uses of the data is to correlate CFD solutions, the utilization of appropriate grids was necessary. The grids were generated and converted to real traverse locations based on the live location of the model in the wind tunnel. This requirement can be challenging for a highly loaded model with significant deflections.

Test Facility

The wind-tunnel test was performed in the 6 ft $\times$ 9 ft subsonic wind tunnel at IAR in Ottawa. It is closed-circuit continuous flow wind tunnel with a maximum speed of approximately 400 ft/sec. The tunnel is equipped with a six-component floor balance, compressed air supply, power supply, cooling water supply and a computer controlled data acquisition and data reduction system.

Model Installation

The two-dimensional wing was installed vertically, spanning the 6 ft dimension of the wind tunnel. The wing was cantilevered from the wind-tunnel balance which is located beneath the floor of the wind tunnel. End plates, isolated from the wind-tunnel balance, were added to improve the two-dimensionality of the flow over the wing. The nacelle was installed mid-span on the wing with the thrust line at a downtilt of 2 degrees relative to the wing chord line. A front view of the the complete model, installed in the wind tunnel, is shown in Figure 2. The traversing rig is also visible in the background.

α deg.	U ft /sec	M	β deg.	Prop RPM	J	C_T	C_P
0.0	335	0.294	60	3100	3.24	0.384	1.596
5.0	200	0.175	32	6000	1.00	0.300	0.423

Table 1: Summary of traversing test conditions.

Traverse Station	Distance Downstream of prop (in)	Description of Traversing Plane
1	2.14	Intake
2	25.27	Wing leading edge
3	35.84	Wing mid-chord
4	45.65	Wing trailing edge (2 in aft)
5	57.03	Nozzle exhaust
6	65.18	Aft of Nacelle

Table 2: Summary of traversing stations.

Test Conditions

Five-hole probe measurements were taken at the two conditions shown in Table 1. The first condition represents a cruise condition and the second represents a climb condition shortly after takeoff. The thrust and power coefficients in the table were measured values from the rotating propeller balance.

Five-hole probe measurements were taken at the six planes shown in Table 2. The location of the planes with respect to the nacelle and wing can be seen in Figure 1. For the cruise condition stations 1,2,4 and 6 were measured. For the takeoff climb condition, all six planes were measured.

Data Acquisition and Reduction

Computer controlled data acquisition, online data reduction, plotting and post-processing of results were provided at the wind tunnel by the Institute for Aerospace Research.

For the five-hole probe measurements, the data from the pressure transducers were digitized, averaged and stored electronically. The sampling rate was 50 samples per second and two seconds of data were taken at each point. At the end of a complete map, which typically required 6 runs, the data were post-processed to apply the five-hole probe calibrations and produce plots. On-line data reduction and plotting was available for these data but not used to maximize the rate of data acquisition. Other data were processed as they were acquired.

Results and Discussion

Wing Surface Pressures

The propeller slipstream has a significant effect on the wing surface pressure distribution. The effect was most dramatic at approximately 70% of the propeller radius, where the propeller blade loading was highest. In this experiment, the propeller rotation was clockwise when viewed from behind the propeller. Consequently, the slipstream swirl results in a decrease in wing loading on the starboard side and an increase on the port side.

The effect of the slipstream for the cruise condition with $\alpha = 0°$ is shown in Figure 3. The pressure distributions for the port and starboard sides match for propeller off. With the propeller on, there was increased suction on the upper surface of the port side and decreased suction on the starboard side. The effect was most noticeable near the leading edge.

For the takeoff climb case, Figure 4, the effect of the slipstream on the pressure distribution was more dramatic. On the port side, the suction peak was much higher than the starboard side. Also, for this case, the suction on the starboard side at mid-chord has increased relative to the propeller-off case due to the increase in dynamic pressure in the slipstream.

The differential integrated lift between port and starboard was shown to be related to the propeller slipstream parameter C_P/J^2, as shown in Figure 5. This parameter is directly related to the slipstream swirl, as was established by Ohman, Nguyen and Barber [5]. To illustrate the direct linear relationship a selection of data points covering a wide range of blade angle and advance ratio J for tests utilizing both a four- and six-blade propeller configurations are shown. At low speeds, where small J values occur in conjunction with high propeller power coefficients very large differential lift coefficients occur as shown in Figure 6. Fortunately when local lift coefficients above 6 are developed the aircraft is still on

the ground!

Traverse Data: Cruise Case

In order to understand the slipstream flow field extent and interaction with the nacelle/wing arrangement, contour plots of total pressure coefficient were plotted for each survey station. Included in the plots are velocity vectors showing the cross-flow magnitude and direction. In all the contour and vector plots, the view is looking upstream and from this viewpoint the propeller is rotating in the clockwise direction.

The first example, for the cruise configuration, is given in Figure 7. This station was immediately behind the propeller at the highlight plane of the inlet. The lower nacelle interferes with the slipstream swirl on the starboard side and little asymmetry is evident. Note, that for this cruise configuration the upwash effect on the propeller was small since the nacelle was tilted down 2 degrees relative to the wing. At the wing leading edge, the upwash enhances the swirl on the port side and detracts from that on the starboard side, Figure 8. Weak flow was developing from the bottom port side of the nacelle.

In Figure 9, at the trailing edge station, the slipstream has been sheared with a significant wake on the port side reflecting the increase in local wing lift. Whilst the slipstream has spread to starboard on the upper surface and to port on the lower surface it was essentially intact but with general weakness along the nacelle port side as indicated by low dynamic pressure and lack of swirl. An enlarged view of the flow field about the aft station is shown in Figure 10. The jet exhaust exhibits some distortion in shape due a bend prior to the exhaust nozzle. The wake from the nacelle appeared significant and biased with weakness in the flow on the port side of the nacelle. Although wing/nacelle junction flows were evident, the dynamic pressure of the flow therein was approximately equal to the freestream. Also, the exhaust tended to expand into the vortices shed by the junction.

Traverse Data: Takeoff Climb Case

In the takeoff climb case, Figure 11, immediately behind the propeller, high levels of distortion were present at the intake plane with a variation in Cpt from 2.8 to 1.6 both circumferentially as well as radially. The intake caused severe distortion in swirl and total pressure. Ahead of the wing leading edge the slipstream may be described as compact with some change in azimuth of the maximum Cpt levels, Figure 12.

At the wing mid-chord station, Figure 13, some widening of the slipstream occurred with the wing shearing action on the rotating stream with some reduction in circumferential distortion. At the trailing edge the contraction of the wing wake was evident at the interface with the slipstream which has spread laterally along the wing from about 0.9 R to about 1.1 R or more on the starboard side, Figure 14. The general form of the slipstream was otherwise intact but a large vortex appears present on the port side of the nacelle due to the slipstream rotation about the deep nacelle. At the exhaust plane, shown in Figure 15, the influence of the exhaust was apparent with some entrainment by the jet with some local reduction in in slipstream swirl. The slipstream retains the form established at the wing trailing edge.

Aft of the nacelle, Figure 16, the flow within the confines of the slipstream was above the freestream dynamic pressure indicating a coalescing of the wing/nacelle wakes and exhaust jet with the slipstream has been achieved with a resulting improvement in propulsive efficiency. Residual existence of the wing/nacelle vortex on the port side where the wing lift has been augmented was displayed. Less ovality of the exhaust jet was evident compared with the cruise case and the nacelle base had minimal impact on the local dynamic pressure, but a reduction in swirl on the the nacelle port side was evident.

Conclusions

Significant changes in local wing upwash occur within the slipstream of a high-speed turboprop. Special requirements on the wing design are necessary to fully exploit the slipstream interaction whilst ensuring wing section compatibility at all flight conditions.

A correlation between local wing lift and the propeller slipstream parameter C_P/J^2 was determined.

This may be used as a valuable criterion in the assessment of local wing sectional requirements in the propeller slipstream.

Valuable data were acquired for understanding the interaction of flows about a turboprop nacelle/wing arrangement. Surface pressure tappings alone do not provide an adequate perspective on flows about a turboprop installation to ensure satisfactory aerodynamic analysis. Flow field data, such as the data presented herein, are required.

The data acquired provides a necessary basis for CFD validation and correlation work on high performance turboprop aircraft. Many existing codes require validation to assess the combination of flows present in a turboprop installation.

Acknowledgements: The wind-tunnel tests were performed in collaboration with Institute of Aerospace Research. This research was performed as part of a shared funded program with Industry Canada. The participation of N. Ball of IAR, R. Fullerton, M. Abramian and N. Choi of de Havilland Inc. is gratefully acknowledged.

References

1. Samuelsson, I., "Experimental investigation of low speed model propeller slipstream aerodynamic characteristics including flow field surveys and nacelle/wing static pressure measurements," in *Proceedings of ICAS 22th Congress*, pp. 71–84, 1990. ICAS 90-3.1.3.

2. Aljabri, A. S., and Hughes, A. C., "Wind tunnel investigation of propeller slipstream interaction with nacelle/wing/flap combinations." AGARD CP-366, Paper 21, February 1985. AGARD Symposium on Aerodynamics and Acoustics of Propellers, Oct. 1984.

3. Eggleston, B., "Some considerations in propeller and airframe integration." AGARD CP-366, Paper 18, February 1985. AGARD Symposium on Aerodynamics and Acoustics of Propellers, Oct. 1984.

4. Smith, B. A. W., "The flow over a wing/nacelle combination in the presence of a propeller slipstream," in *Proceedings of CASI 1st Symposium on Aerodynamics*, pp. 17–1 to 17–17, 1989.

5. Ohman, L.H., Nguyen, V. D., and Barber, D. J., "Probe interference on flow measurements in propeller near slipstream," *Journal of Aircraft*, vol. 32, pp. 887–888, July-August 1995.

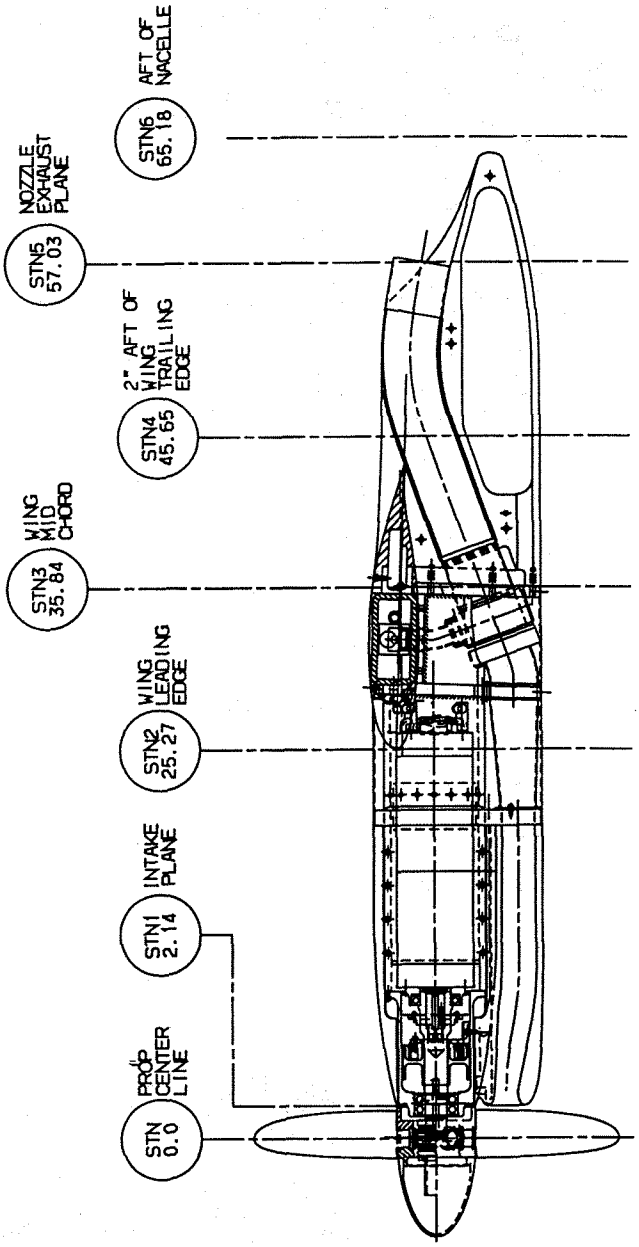

Figure 1: Cross-section through the centerline of the nacelle.

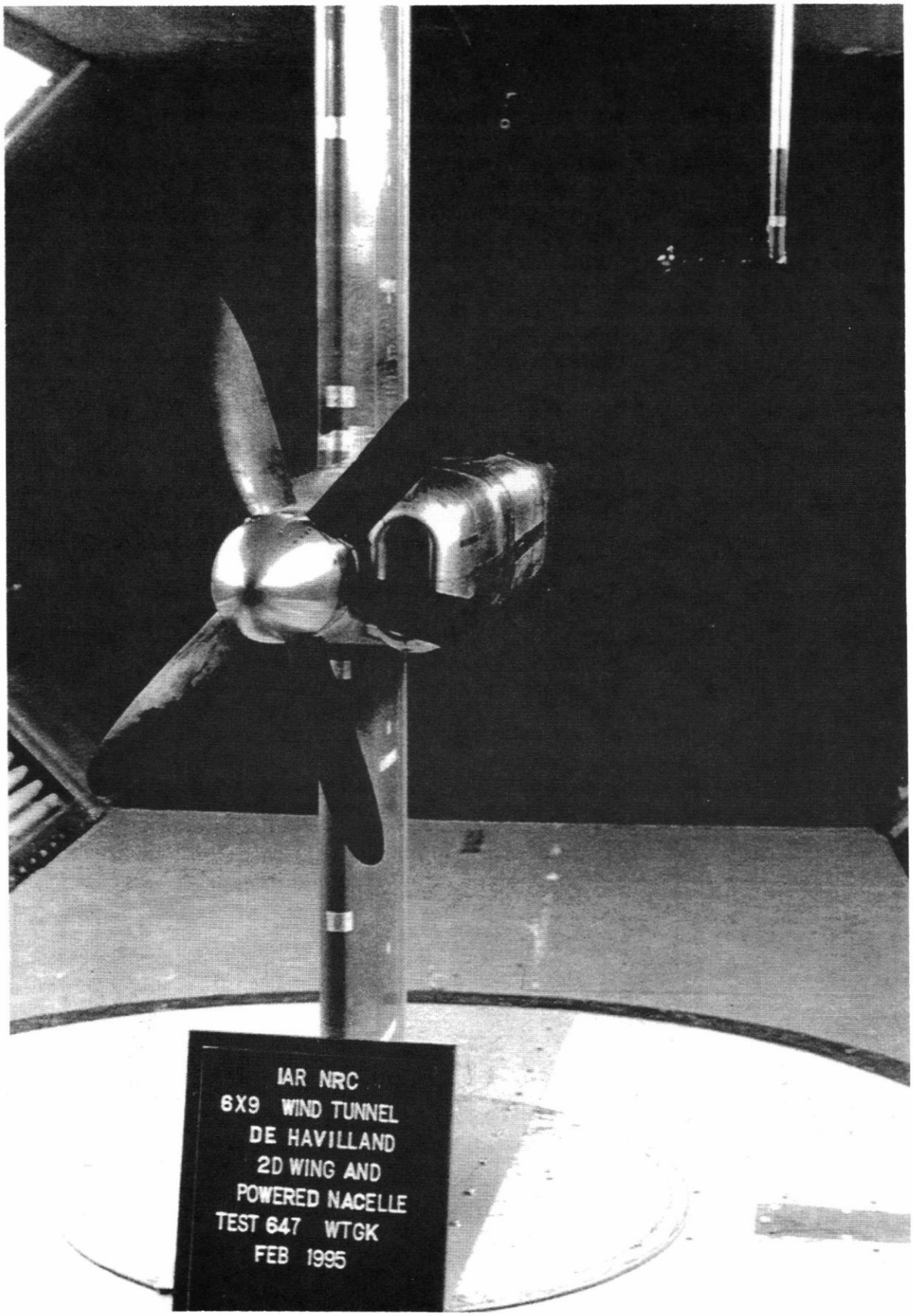

Figure 2: de Havilland wind-tunnel model with nacelle and 6-bladed propeller.

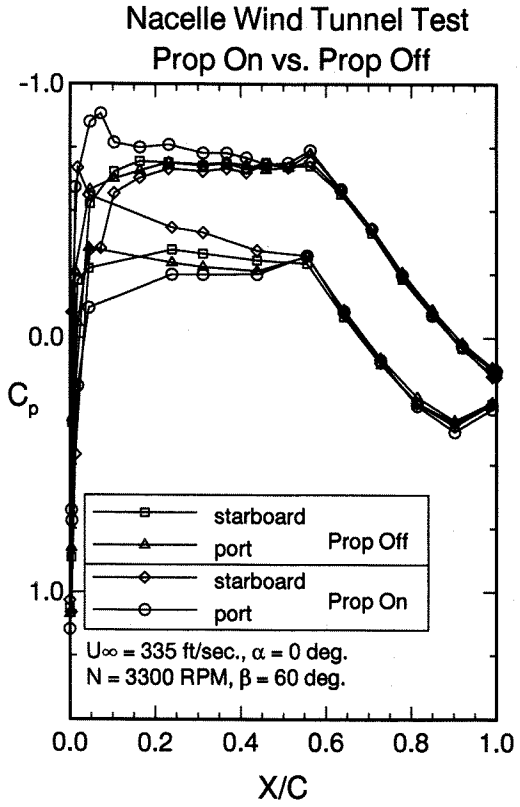

Figure 3: Effect of the propeller slipstream on the wing pressure distribution at $y = \pm 0.7R$, cruise condition, $\alpha = 0°$.

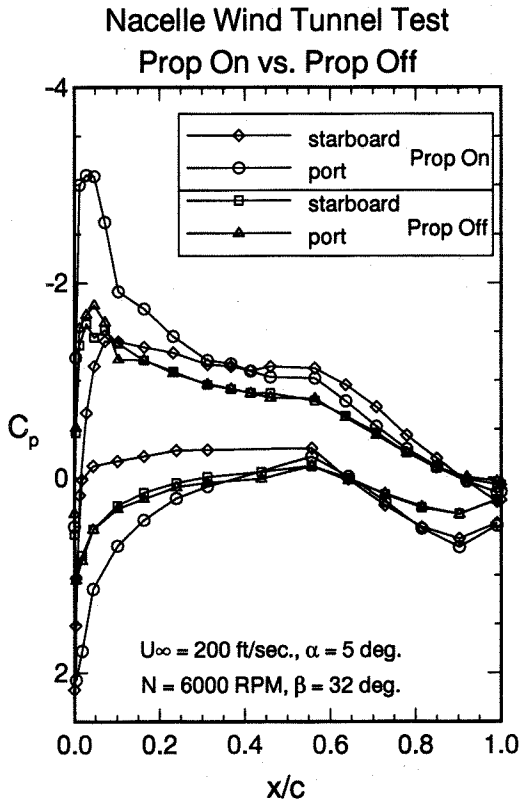

Figure 4: Effect of the propeller slipstream on the wing pressure distribution at $y = \pm 0.7R$, takeoff climb condition, $\alpha = 5°$.

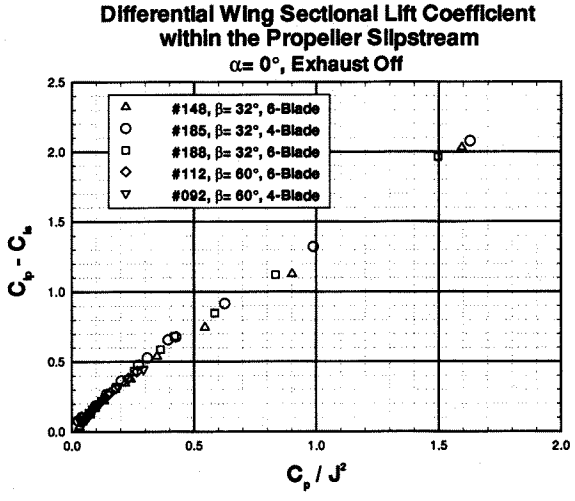

Figure 5: Effect of swirl on wing sectional lift for various blade angles and a large range of J.

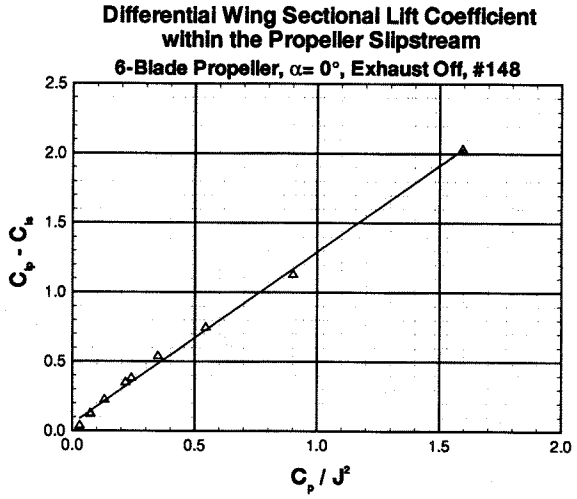

Figure 6: Effect of swirl on wing sectional lift for low J.

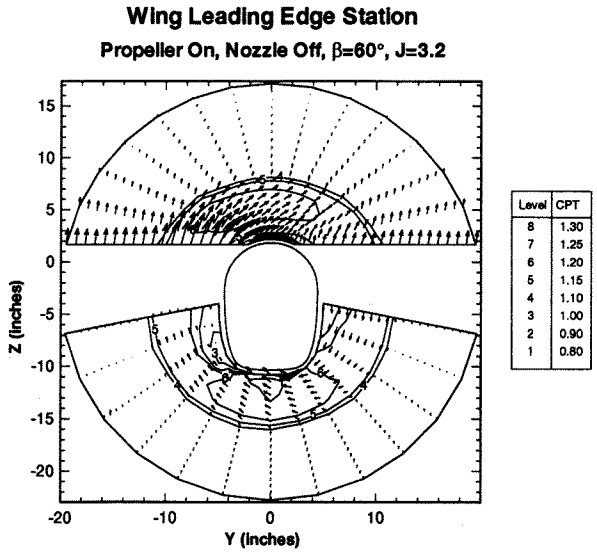

Figure 8: Velocity vectors and contours of total pressure coefficient at station 2 for the cruise condition.

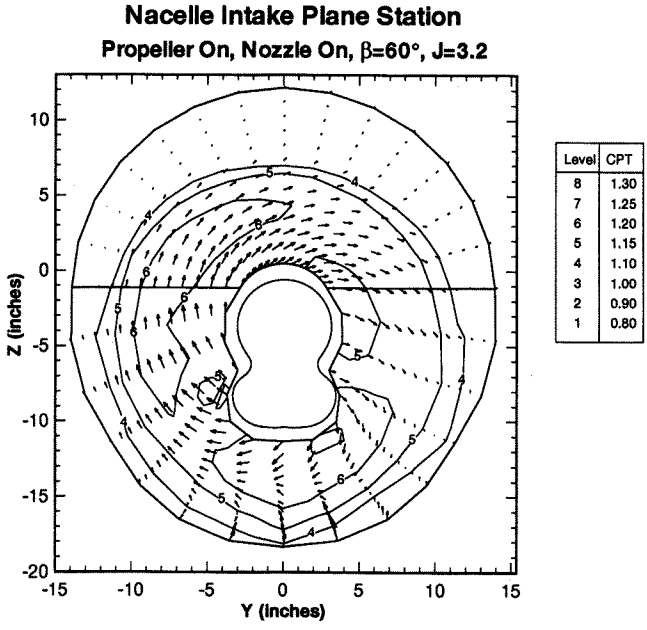

Figure 7: Velocity vectors and contours of total pressure coefficient at station 1 for the cruise condition.

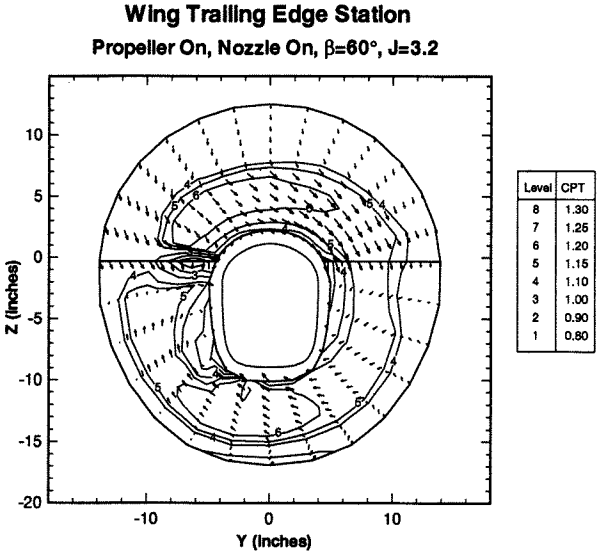

Figure 9: Velocity vectors and contours of total pressure coefficient at station 4 for the cruise condition.

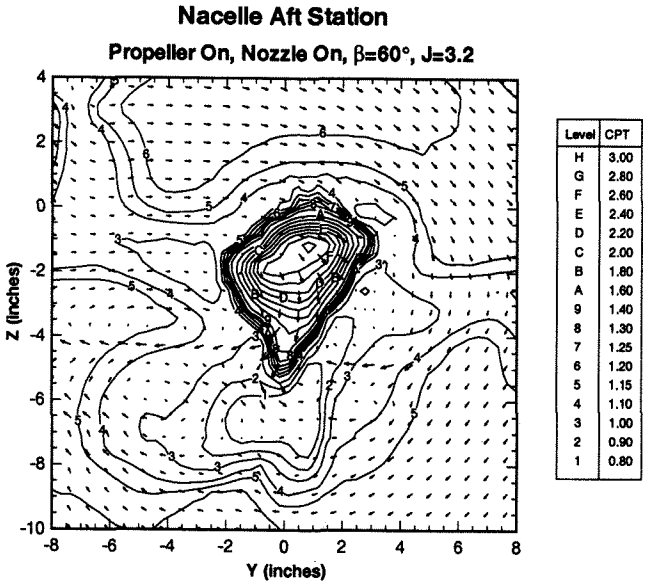

Figure 10: Velocity vectors and contours of total pressure coefficient at station 6 for the cruise condition.

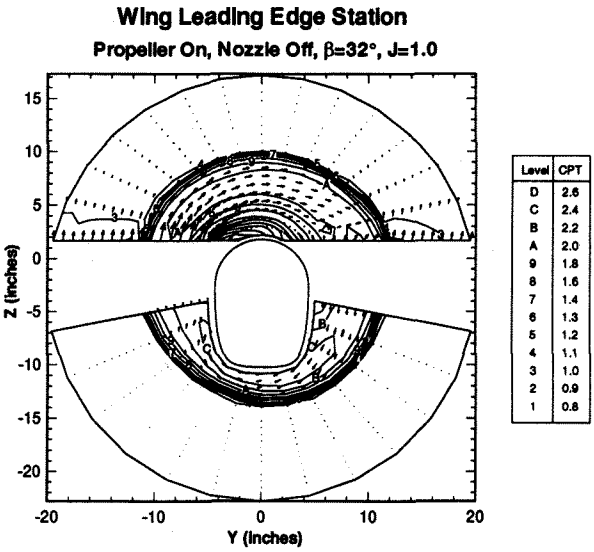

Figure 12: Velocity vectors and contours of total pressure coefficient at station 2 for the takeoff climb condition.

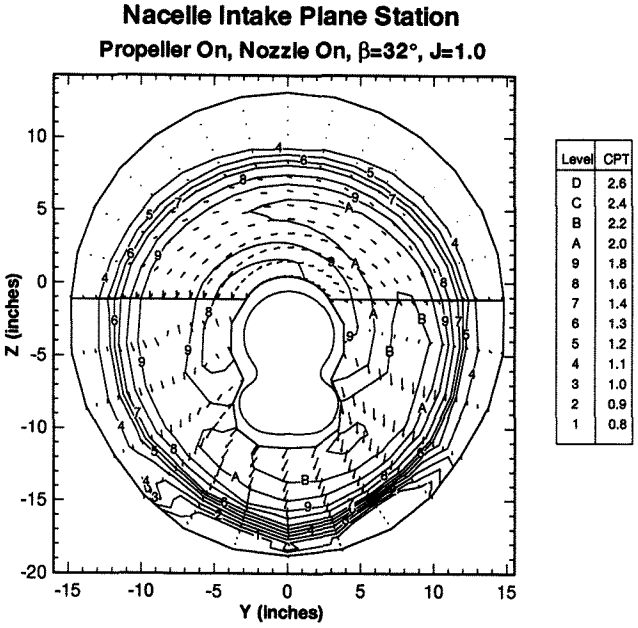

Figure 11: Velocity vectors and contours of total pressure coefficient at station 1 for the takeoff climb condition.

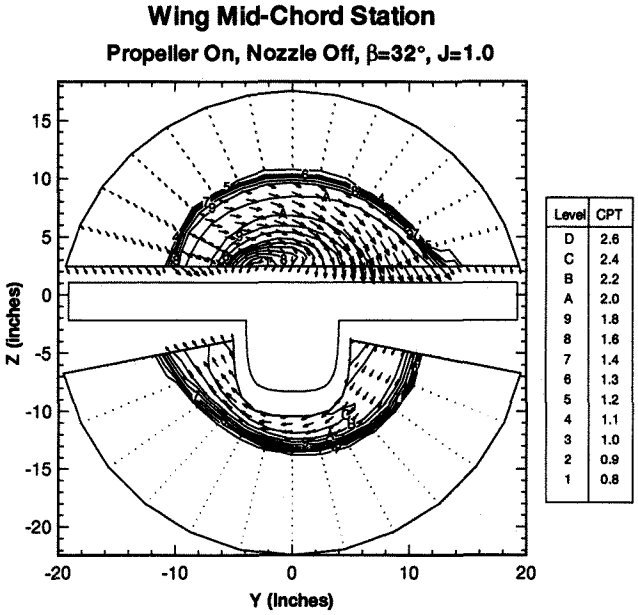

Figure 13: Velocity vectors and contours of total pressure coefficient at station 3 for the takeoff climb condition.

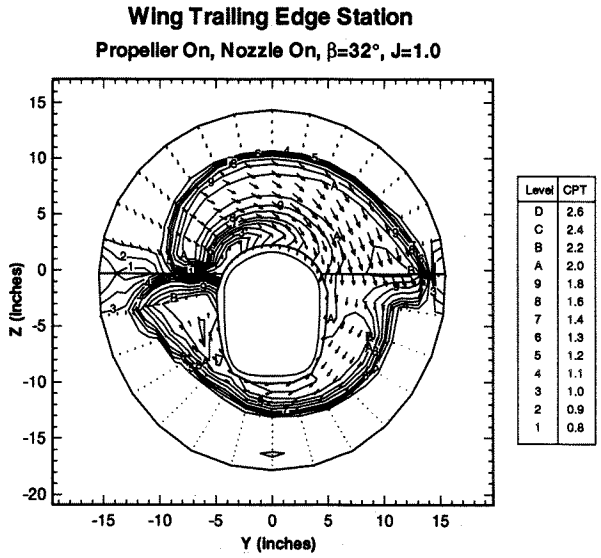

Figure 14: Velocity vectors and contours of total pressure coefficient at station 4 for the takeoff climb condition.

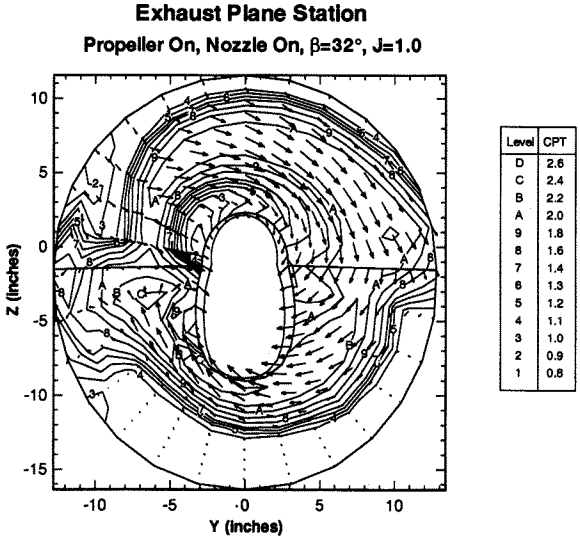

Figure 15: Velocity vectors and contours of total pressure coefficient at station 5 for the takeoff climb condition.

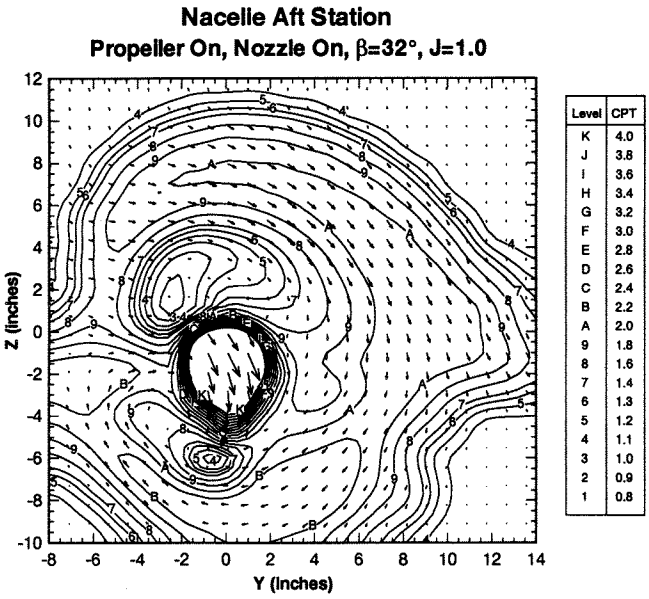

Figure 16: Velocity vectors and contours of total pressure coefficient at station 6 for the takeoff climb condition.